Journal of Power Sources 196 (2011) 8618–8624

Contents lists available at ScienceDirect

Journal of Power Sources

journal homepage: www.elsevier.com/locate/jpowsour

Superior electrode performance of mesoporous hollow TiO_2 microspheres through efficient hierarchical nanostructures

Feng Zhang, Yu Zhang, Shuyan Song, Hongjie Zhang*

State Key Laboratory of Rare Earth Resource Utilization, Changchun Institute of Applied Chemistry, Chinese Academy of Sciences, 5625 Renmin Street, Changchun, Jilin 130022, PR China

ARTICLE INFO

Article history:
Received 25 March 2011
Received in revised form 22 May 2011
Accepted 2 June 2011
Available online 12 June 2011

Keywords:
Lithium-ion battery
Hollow
Hierarchical nanostructures
Controlled

ABSTRACT

Mesoporous hollow TiO_2 microspheres with controlled size and hierarchical nanostructures are designed from a process employing in suit template-assisted and hydrothermal methods. The results show that the hollow microspheres composed of mesoporous nanospheres possess very stable reversible capacity of 184 mAh g^{-1} at 0.25*C* and exhibit extremely high power of 122 mAh g^{-1} at the high rate of 10*C*. The superior high-rate and high-capacity performance of the sample is attributed to the efficient hierarchical nanostructures. The hollow structure could shorten the diffusion length for lithium ion in the microspheres. The large mesoporous channels between the mesoporous nanospheres provide an easily-accessed system which facilitates electrolyte transportation and lithium ion diffusion within the electrode materials. The electrolyte, flooding the mesoporous channels, can also lead to a high electrolyte/electrode contact area, facilitating transport of lithium ions across the electrolyte/electrode interface. The small mesopores in the meosporous nanospheres can make the electrolyte and lithium ion further diffuse into the interior of electrode materials and increase electrolyte/electrode contact area. The small nanoparticles can also ensure high reversible capacity.

© 2011 Elsevier B.V. All rights reserved.

1. Introduction

Due to the ever-increasing demand for powering electric vehicles and portable electronic devices, technological improvements in rechargeable lithium-ion batteries with both high energy and high power densities have been greatly promoted [1–3].

Recent researches indicate that TiO_2 is a potential alternative anode for lithium-ion batteries, since this material is abundant, low-cost, and environment-friendly. Besides, there are nearly no lattice changes during Li^+ insertion/extraction in TiO_2 based structure, which can enhance structural stability and prolong the cycle life [4,5]. However, the charge/discharge rate of bulk TiO_2 material is greatly limited due to the poor ionic and electronic conductivity. Aiming at solving this problem, many studies have been carried out focusing on increasing mixed conduction, including doping the materials with heteroatoms or admixing electronically conductive phases [6–8]. Many materials have been successfully prepared and demonstrated an improved high-rate performance [9–11]. However, these materials usually require noble metals and oxides, or carbon nanotubes and involve complicated preparation, increasing the cost of the active materials.

In the past decades, the development of nanotechnology has brought the anode material researches into a new era. A lot of researches indicate that reducing the dimensions of the electrode materials from micrometer to nanometer can improve the rate performance [12–14]. Nevertheless, there are still shortcomings. For one thing, the nanosized materials make electrode fabrication more difficult than that for micrometer sized materials. For another, it is more difficult to maintain electron pathways between the current collector and the active materials, owing to more contacts that must be preserved against a background of nanosized particles [15]. To acquire an optimized alternative to employ nanoparticles, nanostructured electrode materials have been developed [10,11,16–18]. The unique properties, originating from the nanostructures of those materials, usually give rise to a novel mode to overcome the limitations of conventional nanosized and bulk materials. Consequently, nanostructured electrode materials have drawn a considerable amount of attention as a crucial candidate for the next generation of lithium battery anodes. Up to now, many nanostructured electrode materials have been investigated, including nanotubes, nanoporous materials, nanowires, etc. Among these nanostructured materials, hollow microspheres have received much attention because of their low density, high surface area, strong delivering ability, and effective surface permeability. The template-assisted synthesis is one of the most effective methods to obtain the hollow microspheres [19–22]. Commonly, the template should be synthesized beforehand and then coated with

* Corresponding author. Tel.: +86 431 85262127; fax: +86 431 85262127.
E-mail address: hongjie@ciac.jl.cn (H. Zhang).

0378-7753/$ – see front matter © 2011 Elsevier B.V. All rights reserved.
doi:10.1016/j.jpowsour.2011.06.006

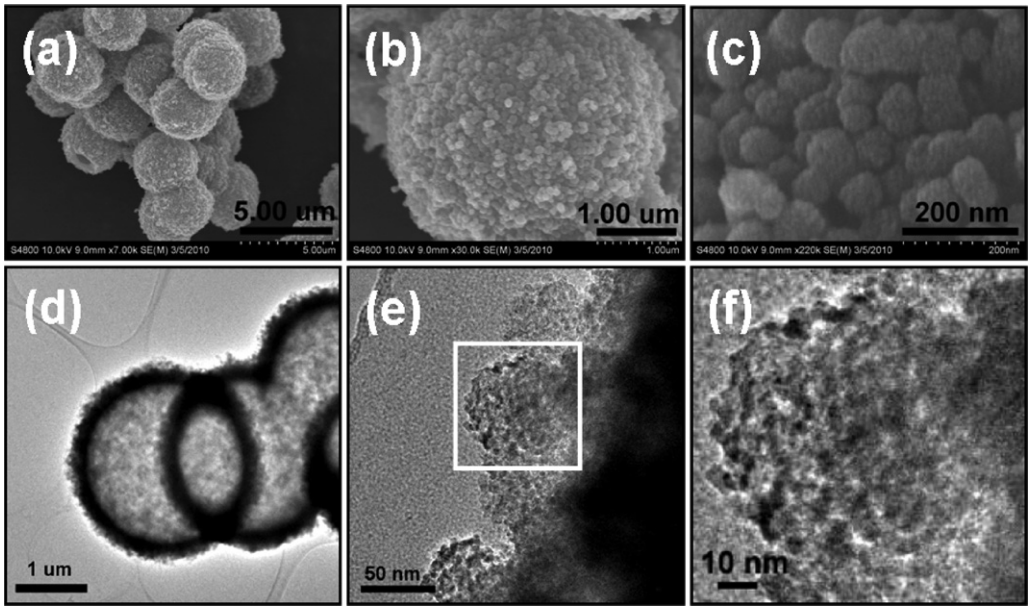

Fig. 1. Scanning electron microscopy (SEM) images (a–c) and transmission electron microscopy (TEM) images (d and e) of TiO_2(48)-400. (f) A magnified TEM image corresponding to the square-marked area (e).

nanoparticles via suitable strategies. This method has several disadvantages, such as difficulty in template fabrication, multistep and costly operations. Recent researches show that the hollow microspheres can also be prepared via solvothermal synthesis, but it generally requires unusual reagents and is strongly affected by several factors, such as the used solvents, the involved ions, and acidity [23–25]. Moreover, the hollow microspheres via the above methods are mostly composed of single nanoparticles. Therefore, it would be desirable to search for a simple synthesis process to synthesize the hollow microspheres with controlled hierarchical nanostructures and size.

In this article, we demonstrate a process that employs both template-assisted and hydrothermal methods for preparation of hollow TiO_2 microspheres with controlled hierarchical nanostructures. The size, composition and hierarchical nanostructures of the obtained hollow microspheres could be easily manipulated via adjusting the hydrothermal reaction time and calcination temperature. Our results show that the hierarchical nanostructures and composition play key roles in electrochemical performance of the TiO_2 hollow microspheres as anode materials. The hollow microspheres composed of mesoporous nanospheres present a superior high-rate and high-capacity performance. The large mesoporous channels between the mesoporous nanospheres facilitate electrolyte transportation and lithium ion diffusion within the electrode materials. The small mesopores in the mesoporous nanospheres can make the electrolyte and lithium ion further diffuse into the interior of electrode materials and increase electrolyte/electrode contact area. The small nanoparticles can also ensure high reversible capacity.

2. Experimental

All chemicals were used as received. A four-step method was adopted in the preparation of TiO_2 hollow microspheres. At first, 5.0 g of titanium sulfate ($Ti(SO_4)_2$) and 0.8 g of resorcinol were dissolved in 30 mL of deionized water. Subsequently, 2.0 mL of 35 wt% formaldehyde was added to the mixture under vigorous stirring and the solution was transferred to a 45 mL Teflon-lined stainless steel autoclave. After heated in an electric oven at 85 °C for 1–48 h, the autoclave was cooled down naturally. The red intermediate products were collected, then washed with deionized water several times, and then dried at 85 °C for a few hours. Finally, the intermediate products were calcined at elevated temperature for 4 h in air to produce the final products. The products were denoted as TiO_2(n)-T, where n and T are the hydrothermal reaction time and calcination temperature.

The transmission electron microscopy (TEM) was performed on a JEOL JEM 3010 electron microscope operating at 300 kV, whereas the scanning electron microscopy (SEM) was carried out on a Hitachi's S-4800 FE-SEM operating at 10.0 kV. The powder X-ray diffraction (XRD) patterns were recorded on a Rigaku XRD spectrometer with Cu Kα radiation (λ = 1.5418 Å). The N_2 adsorption/desorption measurements were performed on a Micromeritics TriStar 3000 system. The surface area data was calculated on the basis of the Brunauer–Emmett–Teller (BET) model whereas the pore size distribution (PSD) was obtained through the Barrett–Joyner–Halenda (BJH) approach.

The electrode was prepared by mixing the final product (80 wt%), acetylene black (10 wt%), and polyvinylidene fluoride (10 wt% PVDF) in N-methylpyrrolidone (NMP) into a homogenous slurry. The slurry was then spread onto a copper foil and dried at 100 °C for 24 h in a vacuum oven. 1 M $LiPF_6$ in a mixture of ethylene carbonate (EC), dimethyl carbonate (DMC) and ethyl methyl carbonate (EMC) (1:1:1 by weight) was used as the electrolyte. The assembly of the test cells was carried out in an argon-filled glove box. The batteries were charged and discharged at the rate of 0.25C, 1.5C and 2.25C (1C = 335 mAh g^{-1}) between 1.0 and 3.0 V on a LAND CT2001A cell test apparatus. Furthermore, the electrode charged and discharged at high rate of 2.5C, 5C and 10C was composed of the final product (60 wt%), acetylene black (20 wt%), and polyvinylidene fluoride (20 wt%).

3. Results and discussion

The morphology and structure of TiO_2(48)-400 are examined by SEM and TEM. Fig. 1a and d presents the low-magnification SEM and TEM images of TiO_2(48)-400, it is obvious to see that the sample mainly contains uniform hollow microspheres with a diameter of approximately 3.4 μm. The SEM images with high magnification (Fig. 1b and c) show that the hollow microspheres are composed

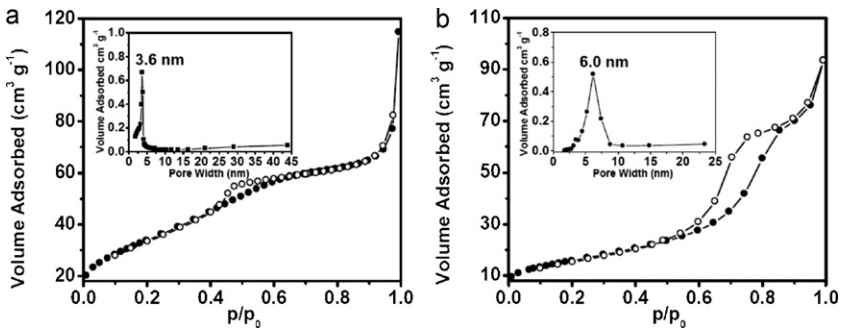

Fig. 2. Nitrogen adsorption/desorption isotherms measured at 77 K from (a) TiO_2(48)-400 and (b) TiO_2(48)-550 with corresponding pore size distributions calculated by Barrett–Joyner–Halenda (BJH) method from each branch.

of a lot of nanospheres. These nanospheres are around 60 nm in diameter and assembled in an irregular manner, leaving plenty of mesoporous channels between the nanospheres. The texture of the nanospheres is further identified by the TEM images. As shown in Fig. 1e and f, the nanospheres consist of some TiO_2 nanoparticles with a diameter of about 6 nm and a considerable amount of mesopores with the diameter of 3–4 nm are present. On the basis of the SEM and TEM observations, TiO_2(48)-400 are considered to be hierarchical nanostructures.

The mesoporous feature of TiO_2(48)-400 is further confirmed by nitrogen adsorption/desorption isotherm with corresponding pore size distribution as shown in Fig. 2a. The isotherm is characteristic of type-IV adsorption curve, displaying the existence of mesopores in the obtained hollow microspheres [26]. Fig. 2a displays the BJH pore size distribution (PSD) and it is seen that the majority of the mesopores in TiO_2(48)-400 have diameters of approximately 3.6 nm. The pore size distribution curve also suggests that mesopores larger than 10 nm are present in TiO_2(48)-400, which arise from the accumulation of the nanospheres. The surface area and pore volume of TiO_2(48)-400 are 123 $m^2\,g^{-1}$ and 0.19 $cm^3\,g^{-1}$, respectively. Based on the N_2 adsorption/desorption isotherm and the PSD data, TiO_2(48)-400 contain hierarchical porous structures, in good agreement with the pore sizes observed via TEM images. It is worth noting that the calcination temperature affects the porous structure of the hollow microspheres. Fig. 2b shows the nitrogen adsorption/desorption isotherm and pore size distribution of TiO_2(48)-550. Mesopores still exist in the hollow microspheres, but the size of the mesopores is around 6.0 nm. In addition, the surface area and pore volume of TiO_2(48)-550 reduce to 57 $m^2\,g^{-1}$ and 0.12 $cm^3\,g^{-1}$, respectively, consistent with the N_2 adsorption/desorption analysis results.

The crystallographic structures of the TiO_2(48)-T specimens are confirmed by X-ray powder diffraction (XRD) analysis (Fig. 3). According to the XRD patterns, almost pure anatase TiO_2 (JCPDS 21-1272) is observed after the removal of polymers by calcination below 400 °C, indicating that the phase of TiO_2(48)-400 is mainly composed of anatase. When the calcination temperature is elevated to 550 °C, the weak diffraction peaks indexed to the tetragonal rutile TiO_2 (JCPDS21-1276) structure are observed, illustrating that a low percentage of anatase phase transform into rutile phase. The relative intensities and sharpness of the rutile peaks in the XRD patterns increase with the calcination temperature, which shows that the components of the rutile phase could be controlled via adjusting the calcination temperature.

It is also found that the hydrothermal reaction time has important influence on the morphology of the products. Fig. 4 shows the SEM images of the samples prepared with various hydrothermal reaction times and calcined at 550 °C. When the hydrothermal reaction time is shorter than 12 h, the hollow microspheres are mainly composed of single nanoparticles, and the size and shell thickness increase along with the hydrothermal reaction time. As the hydrothermal reaction time increased to 48 h, the hollow microspheres composed of mesoporous TiO_2 nanospheres are formed. Based on the SEM images, it is concluded that the size, shell thickness, and hierarchical nanostructures of the hollow microspheres can be easily manipulated by adjusting the hydrothermal reaction time.

In order to investigate the formation mechanism of TiO_2 hollow microspheres, the intermediate products are characterized by SEM and XRD (Figs. 5 and 6). The SEM images display that the intermediate products are all spheric in shape, whereas the sizes and the structures of coated TiO_2 nanoparticles vary with the hydrothermal reaction time. In Fig. 5, it shows that amorphous TiO_2 are formed when the reaction time is less than 1 h, since there are no diffraction peaks in the XRD pattern (Fig. 6). However, anatase TiO_2 begins to present as the hydrothermal reaction time extended to more than 2 h. According to these observations, a general scheme of the formation of TiO_2 hollow microspheres is proposed. As shown in Scheme 1, under hydrothermal conditions, the polymer microspheres were formed through the polymerization of resorcinol and formaldehyde. During this process, TiO_2 nanoparticles produced via the hydrolysis of $Ti(SO_4)_2$ simultaneously congregated around the polymer microspheres, forming the core–shell intermediate products. When the hydrothermal reaction time was shorter than 12 h, the amount of TiO_2 nanoparticles around the polymer microspheres increased along with the hydrothermal reaction time, resulting in the increase of the size and shell thickness of the intermediate products. Further increasing the hydrothermal reaction time, the TiO_2 nanoparticles around the polymer microspheres

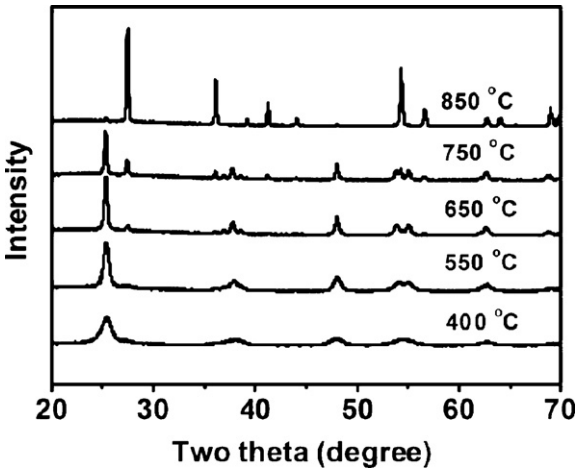

Fig. 3. XRD patterns of TiO_2(48)-*T* specimens. Calcination temperatures (*T*) are marked 400, 550, 650, 750 and 850 °C.

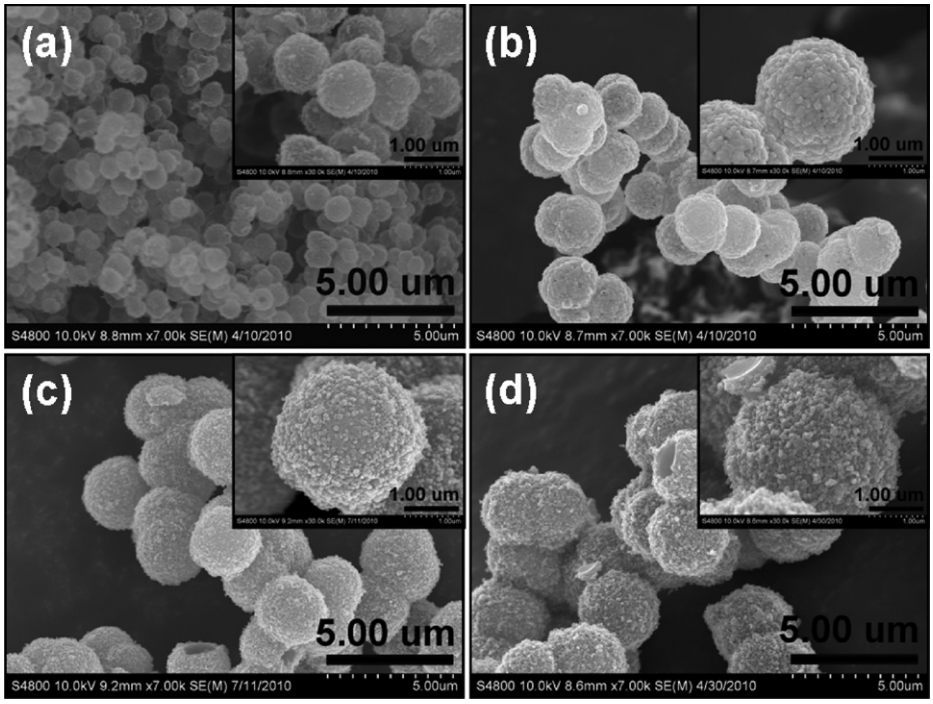

Fig. 4. SEM images of the hollow TiO_2 microspheres prepared for various hydrothermal reaction times and calcined at 550 °C (a: 1 h, b: 2 h, c: 12 h, and d: 48 h).

began to assemble into mesoporous nanospheres. The size, shell thickness and structures of the intermediate products vary with the hydrothermal reaction times, and this is the reason why the structures of the final products could be manipulated by simply adjusting the hydrothermal reaction times. Finally, the polymer was removed from the intermediate products by calcination and TiO_2 hollow microspheres were obtained.

Fig. 7a shows the charge/discharge behaviors for several representative cycles for TiO_2(48)-400 at 0.25*C* rate with a voltage window of 1–3 V. The first charge/discharge curve of TiO_2(48)-400 indicates a discharge capacity of approximately 347 mAh g^{-1} and a charge capacity of 230 mAh g^{-1}. The reversible capacity of 230 mAh g^{-1} ($Li_{0.69}TiO_2$) is close to the theoretical capacity of TiO_2 ($LiTiO_2$, 335 mAh g^{-1}). It is attributed to the existence of lots of mesopores in TiO_2(48)-400, which could increase lithium storage capacity [16,27]. The high irreversible capacity in the region before a constant-voltage plateau (>1.75 V) and low coulombic efficiency, which are common for TiO_2-based materials, is attributed to the Li surface storage in nanostructured TiO_2 to form the conductive Li_xTiO_2 in the solid-solution domain [19,28–30]. Although the coulombic efficiency of the first cycle is low, it is improved upon cycling. The shape of the charge/discharge curves from the

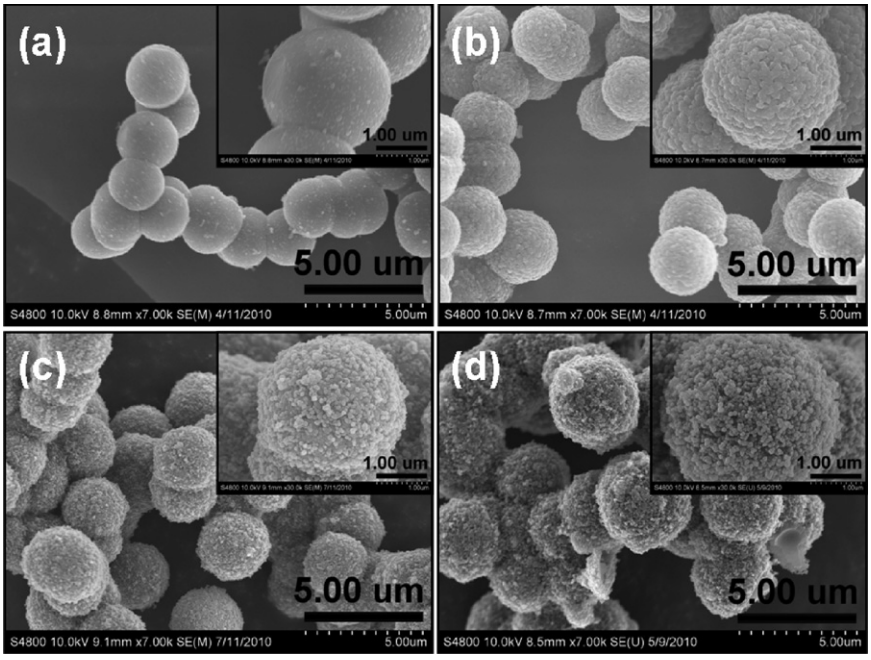

Fig. 5. SEM images of the intermediate products prepared for various hydrothermal reaction times (a: 1 h, b: 2 h, c: 12 h, and d: 48 h).

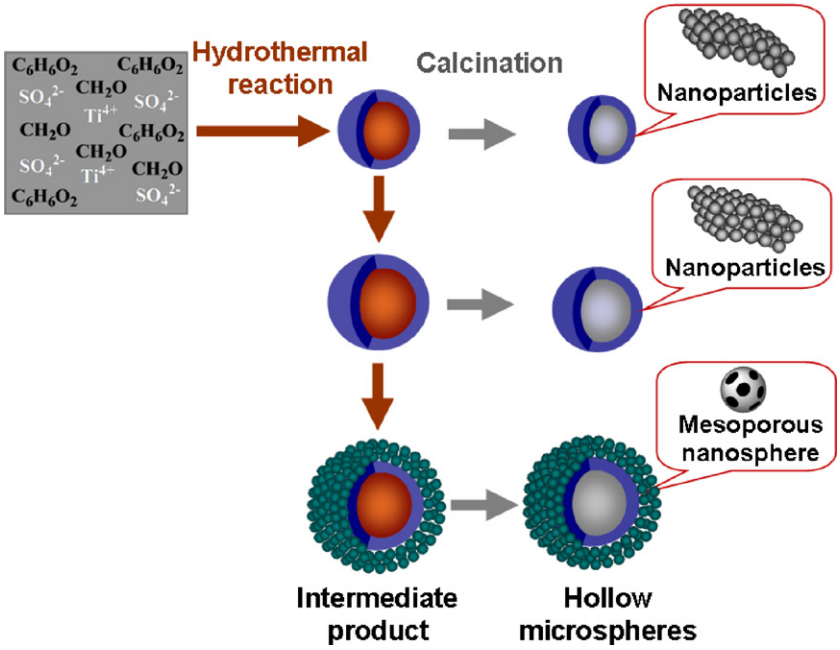

Scheme 1. Schematic illustration of the formation of the mesoporous hollow TiO_2 microspheres with hierarchical nanostructures.

second cycle is rarely changed with discharge and charge potential plateaus at about 1.8 and 1.9 V. Fig. 7b presents the cycling performance of TiO_2(48)-400 at 0.25*C* and 1.5*C* rate. Obviously, TiO_2(48)-400 possess excellent cycling performance over extended cycling, and they are able to give a reversible capacity of 184 ($Li_{0.55}TiO_2$) and 172 mAh g^{-1} ($Li_{0.51}TiO_2$) after 40 cycles, respectively.

In order to elucidate the effect of hierarchical nanostructures on the rate capability of hollow microspheres, TiO_2(12)-400 and TiO_2(48)-400 with different hierarchical nanostructures are tested under the same condition. For comparison, the TiO_2 nanoparticles prepared without resorcinol and formaldehyde for 48 h and calcination at 400 °C for 4 h are also tested under the same condition (Fig. 8a). As is seen, both of the hollow microspheres show superior cycling performance over extended cycling, and give larger reversible capacities than that of TiO_2 nanoparticles after 40 cycles even at high rate of 2.25*C*. It indicates that hollow structures can obviously improve the electrochemical property of nanoparticles. However, the electrochemical performances of hollow micro-

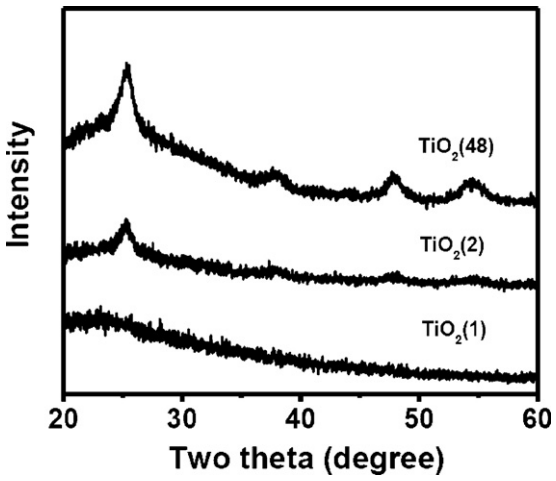

Fig. 6. XRD patterns of intermediate products prepared for various hydrothermal reaction times.

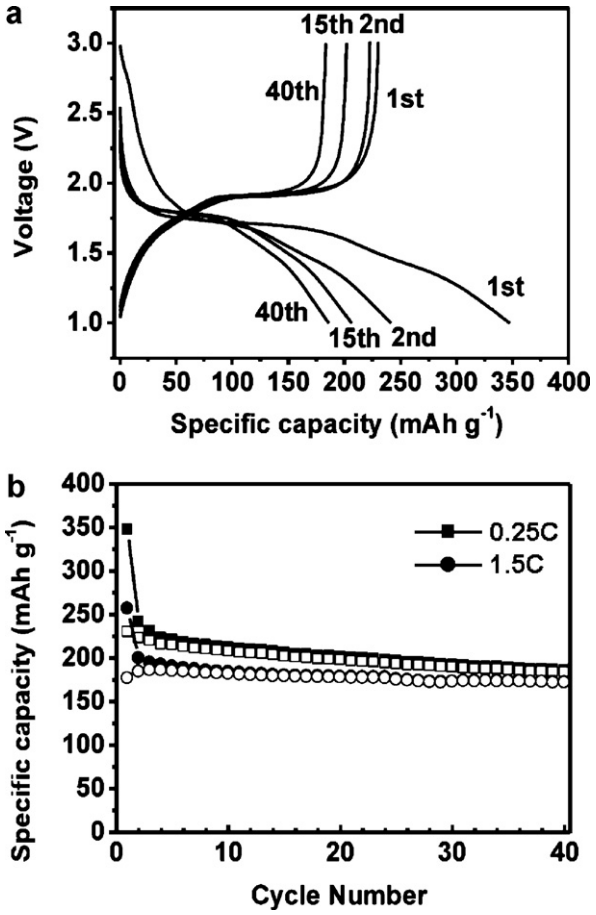

Fig. 7. (a) The charge/discharge behavior of TiO_2(48)-400 for several representative cycles at 0.25*C* rate with a voltage window of 1–3 V (1st, 2nd, 15th and 40th). (b) Cycling performance of TiO_2(48)-400 at 0.25*C* and 1.5*C*.

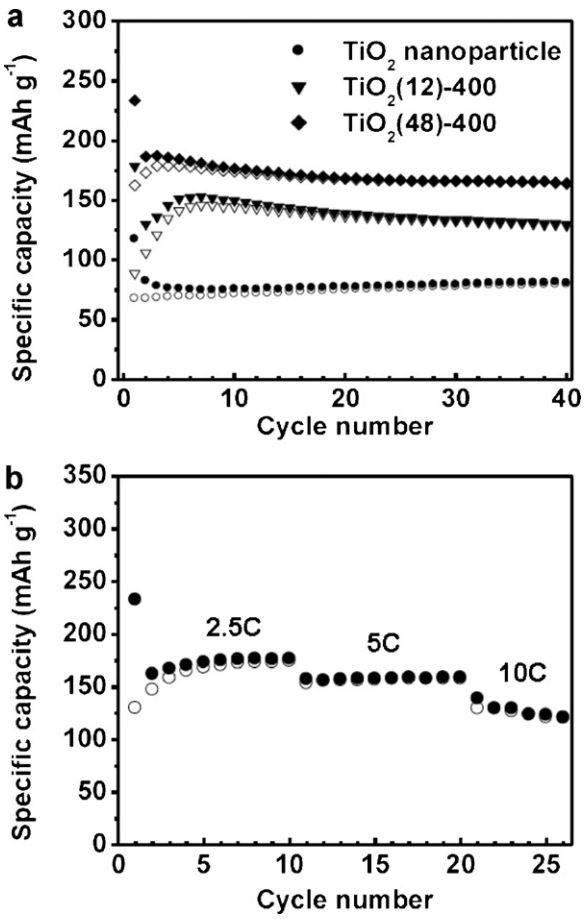

Fig. 8. (a) Cycling performance of TiO_2 nanoparticles, TiO_2(12)-400 and TiO_2(48)-400 at 2.25*C*. (b) Cycling performance of TiO_2(48)-400 at high rates of 2.5*C*, 5*C* and 10*C*.

spheres vary with the hierarchical nanostructures. It is obvious that TiO_2(48)-400 present the better performance. Although the relatively large irreversible loss in the first cycle, the difference between discharge and charge capacity becomes insignificant in the course of first several cycles, and thenceforth the coulombic efficiency is nearly 100%. From this we can see TiO_2(48)-400 have excellent electrochemical performance over extended cycling. It is able to give the reversible capacities of 164 mAh g^{-1} ($Li_{0.49}TiO_2$) after 40 cycles. Additionally, the reversible capacity of TiO_2(48)-400 cycling at high rates is distinctly higher than that of most reported TiO_2 nanostructures and doping TiO_2 materials [11,16,17,19,31]. Furthermore, TiO_2(48)-400 remain relatively high reversible capacities even at higher charge/discharge rates as shown in Fig. 8b. The cell is first cycled at 2.5*C* and the charge/discharge rate is gradually increased to 10*C*. The reversible capacity of approximately 175 mAh g^{-1} is obtained at 2.5*C* after 10 cycles, and this value reduced to about 158 and 122 mAh g^{-1} at the high rates of 5*C* and 10*C*. The reversible capacities of TiO_2(48)-400 at 5*C* and 10*C* can compared with that of mesoporous TiO_2:RuO_2 nanocomposite, in which the oxide RuO_2 act as a suitable electronic conductor to improve surface–surface interactions [9]. The high-rate performance of TiO_2(48)-400 is attributed to the efficient hierarchical nanostructure. As shown in Scheme 2, the hollow structure of TiO_2(48)-400 could shorten the diffusion length for lithium ion in the microspheres. The large mesoporous channels between the mesoporous nanospheres provide an easily-accessed system which facilitates electrolyte transportation and lithium ion diffusion within the electrode materials. The electrolyte, flooding the mesoporous channels, can also lead to a high electrolyte/electrode contact area, facilitating transport of lithium ions across the electrolyte/electrode interface. The small mesopores in the mesoporous nanospheres can make the electrolyte and lithium ion further diffuse into the interior of electrode materials and increase electrolyte/electrode contact area. The small sized nanoparticles can also ensure high reversible capacity [29,32]. All these factors contribute to the high reversible capacity and high-rate performance of our materials.

To investigate the effect of surface area and pore volume of hollow microspheres on electrochemical performance, TiO_2(48)-550 with lower surface area and pore volume have also been used as the electrode materials (Fig. 9). The first charge/discharge curve of TiO_2(48)-550 indicates a discharge capacity of about 297 mAh g^{-1} and a charge capacity of 207 mAh g^{-1} (Fig. 9a). The irreversible capacity is also mainly attributed to the Li surface storage in nanostructured TiO_2 [19,28–30]. However, the capacity of Li surface storage of TiO_2(48)-550 is smaller than that of TiO_2(48)-400. It is mainly due to the smaller surface area of TiO_2(48)-550 [30]. After further cycling for 16 cycles, a reversible capacity of 167 mAh g^{-1} ($Li_{0.5}TiO_2$) still remains. Fig. 9b presents the cycling performance of TiO_2(48)-550 at 1.5*C* rate. It is able to give a reversible capacity of 143 mAh g^{-1} ($Li_{0.43}TiO_2$) after 40 cycles. TiO_2(48)-550 also possess excellent electrochemical performance at 0.25*C* and 1.5*C* rate, but the reversible capacity of TiO_2(48)-550 is distinctly smaller than that of TiO_2(48)-400, indicating the positive correlation between reversible capacity of the materials and the surface area as well as pore volume. Electrolyte transportation and lithium ion diffusion are more available in materials with higher surface areas and larger pore volume, and this might account for the correlation mentioned above.

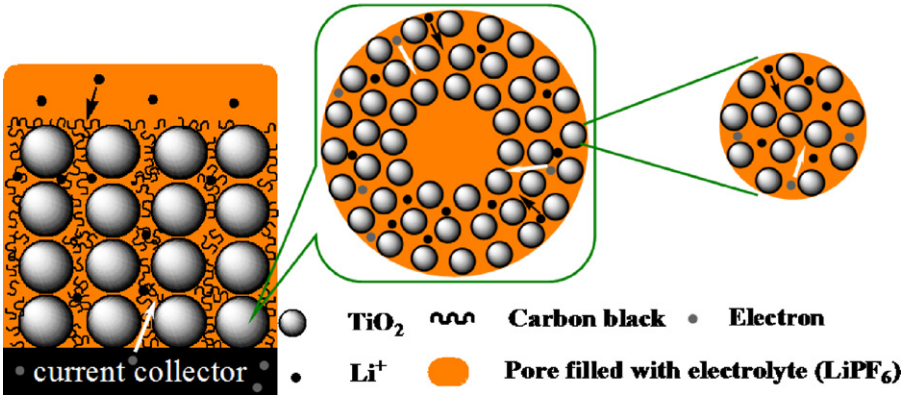

Scheme 2. Schematic representation of lithium insertion into the TiO_2(48)-400.

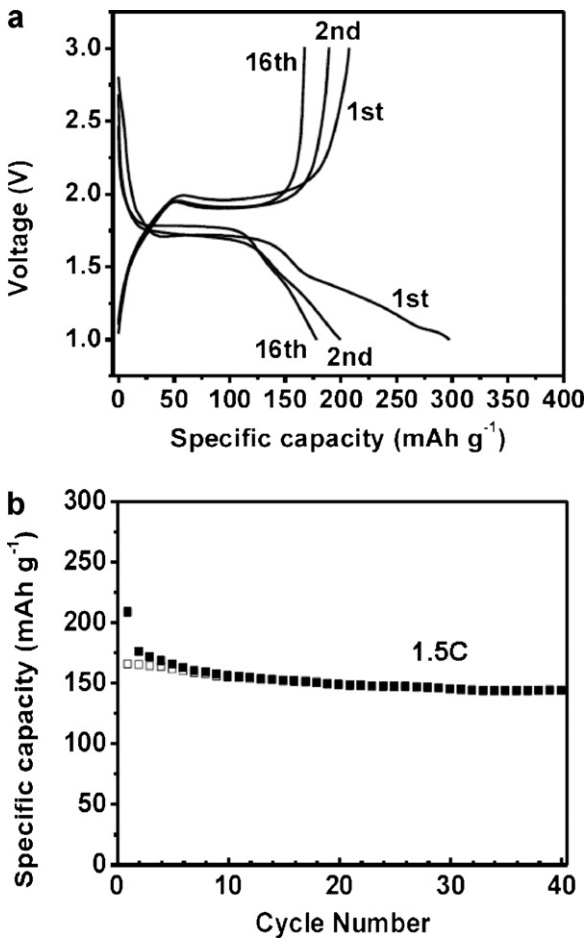

Fig. 9. (a)The charge/discharge behavior of TiO_2(48)-550 for several representative cycles at 0.25*C* rate with a voltage window of 1–3 V (1st, 2nd and 16th). (b) Cycling performance of TiO_2(48)-550 at 1.5*C* rate.

4. Conclusions

TiO_2 hollow microspheres with controlled hierarchical nanostructures were successfully prepared via simple hydrothermal synthesis and calcination. The size, shell thickness, composition and hierarchical nanostructures of the obtained hollow microspheres could be easily manipulated via adjusting the hydrothermal reaction time and calcination temperature. These hollow microspheres exhibit high reversible capacities and good cycling performance when used as anode materials. The electrochemical properties of hollow microspheres vary with the hierarchical nano structures. Our results show that the hollow microspheres composed of mesoporous TiO_2 nanospheres maintain a particularly large reversible capacity even at high charge/discharge rates. During charge/discharge process, the hollow structure and large mesoporous channels of the material facilitate electrolyte transportation and lithium ion diffusion and the small mesopores and small sized nanoparticles increase the lithium storage capacity.

Our approach for the preparation of TiO_2 hollow microspheres with controlled hierarchical nanostructures opens new possibilities for exploitation of suitable anode materials for high-rate and high-capacity lithium-ion batteries.

Acknowledgements

The authors are grateful to the financial aid from the National Natural Science Foundation of China (Grant no. 21071140) and National Natural Science Foundation for Creative Research Group (Grant no. 20921002).

References

[1] H. Zhang, X.P. Gao, G.R. Li, T.Y. Yan, H.Y. Zhu, Electrochim. Acta 53 (2008) 7061–7068.
[2] J.M. Tarascon, M. Armand, Nature 414 (2001) 359–367.
[3] C.H. Lin, C.H. Shen, A.A.M. Prince, S.M. Huang, R.S. Liu, Solid State Commun. 133 (2005) 687–690.
[4] Y.S. Hu, L. Kienle, Y.G. Guo, J. Maier, Adv. Mater. 18 (2006) 1421–1426.
[5] D.H. Lee, J.G. Park, K.J. Choi, H.J. Choi, D.W. Kim, Eur. J. Inorg. Chem. (2008) 878–882.
[6] A.R. Armstrong, G. Armstrong, J. Canales, P.G. Bruce, Angew. Chem. Int. Ed. 43 (2004) 2286–2288.
[7] N. Ravet, Y. Chouinard, J.F. Magnan, S. Besner, M. Gauthier, M. Armand, J. Power Sources 97–8 (2001) 503–507.
[8] R. Dominko, M. Bele, M. Gaberscek, M. Remskar, D. Hanzel, J.M. Goupil, S. Pejovnik, J. Jamnik, J. Power Sources 153 (2006) 274–280.
[9] Y.G. Guo, Y.S. Hu, W. Sigle, J. Maier, Adv. Mater. 19 (2007) 2087–2091.
[10] A. Ghicov, M. Yamamoto, P. Schmuki, Angew. Chem. 120 (2008) 8052–8055.
[11] B.L. He, B. Dong, H.L. Li, Electrochem. Commun. 9 (2007) 425–430.
[12] P.G. Bruce, B. Scrosati, J.M. Tarascon, Angew. Chem. Int. Ed. 47 (2008) 2930–2946.
[13] Y.J. Lee, H. Yi, W.J. Kim, K. Kang, D.S. Yun, M.S. Strano, G. Ceder, A.M. Belcher, Science 324 (2009) 1051–1055.
[14] Y.G. Wang, Y.R. Wang, E. Hosono, K.X. Wang, H.S. Zhou, Angew. Chem. Int. Ed. 47 (2008) 7461–7465.
[15] Y. Ren, A.R. Armstrong, F. Jiao, P.G. Bruce, J. Am. Chem. Soc. 132 (2010) 996–1004.
[16] D.H. Wang, D.W. Choi, Z.G. Yang, V.V. Viswanathan, Z.M. Nie, C.M. Wang, Y.J. Song, J.G. Zhang, J. Liu, Chem. Mater. 20 (2008) 3435–3442.
[17] H. Qiao, Y.W. Wang, L.F. Xiao, L.Z. Zhang, Electrochem. Commun. 10 (2008) 1280–1283.
[18] W.B. Yue, C. Randorn, P.S. Attidekou, Z.X. Su, J.T.S. Irvine, W.Z. Zhou, Adv. Funct. Mater. 19 (2009) 2826–2833.
[19] X.W. Lou, L.A. Archer, Adv. Mater. 20 (2008) 1853–1858.
[20] T.H. Kim, K.H. Lee, Y.K. Kwon, J. Colloid Interface Sci. 304 (2006) 370–377.
[21] L.J. Fu, L.C. Yang, Y. Shi, B. Wang, Y.P. Wu, Micropor. Mesopor. Mater. 117 (2009) 515–518.
[22] R.A. Caruso, A. Susha, F. Caruso, Chem. Mater. 13 (2001) 400–409.
[23] B. Song, S.W. Liu, J.K. Jian, M. Lei, X.J. Wang, H. Li, J.G. Yu, X.L. Chen, J. Power Sources 180 (2008) 869–874.
[24] J.H. Pan, X.W. Zhang, A.J. Du, D.D. Sun, J.O. Leckie, J. Am. Chem. Soc. 130 (2008) 11256–11257.
[25] H.G. Yang, H.C. Zeng, J. Phys. Chem. B 108 (2004) 3492–3495.
[26] M. Kruk, M. Jaroniec, Chem. Mater. 13 (2001) 3169–3183.
[27] F.Y. Cheng, Z.L. Tao, J. Liang, J. Chen, Chem. Mater. 20 (2008) 667–681.
[28] Y.G. Guo, Y.S. Hu, J. Maier, Chem. Commun. (2006) 2783–2785.
[29] C.H. Jiang, M.D. Wei, Z.M. Qi, T. Kudo, I. Honma, H.S. Zhou, J. Power Sources 166 (2007) 239–243.
[30] G. Sudant, E. Baudrin, D. Larcher, J.M. Tarascon, J. Mater. Chem. 15 (2005) 1263–1269.
[31] J.P. Wang, Y. Bai, M.Y. Wu, J. Yin, W.F. Zhang, J. Power Sources 191 (2009) 614–618.
[32] M. Wagemaker, W.J.H. Borghols, F.M. Mulder, J. Am. Chem. Soc. 129 (2007) 4323–4327.